Heterogeneous Diffusion in Highly Supercooled Liquids

Ryoichi Yamamoto and Akira Onuki
Department of Physics, Kyoto University, Kyoto 606-8502, Japan
(Received 13 July 1998)

The diffusivity of tagged particles is demonstrated to be heterogeneous on time scales comparable to or less than the stress relaxation time $\cong \tau_\alpha$ in a highly supercooled model liquid. The particle motions in the relatively active regions dominantly contribute to the mean square displacement, giving rise to a diffusion constant larger than the Stokes-Einstein value. The van Hove self-correlation function $G_s(r,t)$ is shown to have a large r tail which can be scaled in terms of $r/t^{1/2}$ for $t \lesssim 3\tau_\alpha$. Its presence indicates heterogeneous diffusion in the active regions. However, the diffusion process becomes homogeneous on time scales longer than the life time of the heterogeneity structure ($\sim 3\tau_\alpha$). [S0031-9007(98)07758-8]

PACS numbers: 64.70.Pf, 61.43.Fs, 66.10.Cb

In a wide range of liquid states, the Stokes-Einstein relation $D\eta a/k_BT = \text{const}$ has been successfully applied between the translational diffusion constant D of a tagged particle and the viscosity η even when the tagged particle diameter a is of the same order as that of solvent molecules. However, this relation is systematically violated in fragile supercooled liquids [1–6]. The diffusion process in supercooled liquids thus remains not well understood. In particular, Sillescu *et al.* observed the power law behavior $D \propto \eta^{-\nu}$ with $\nu \cong 0.75$ at low temperatures [2]. Furthermore, Ediger *et al.* found that smaller probe particles exhibit a more pronounced increase of $D\eta/T \propto D/D_{\rm SE}$ with decreasing T [3], where $D_{\rm SE} \sim k_BT/2\pi\eta a$ is the Stokes-Einstein diffusion constant. In such experiments the viscosity changes over 12 decades with decreasing T, while the ratio $D/D_{\rm SE}$ increases from order 1 up to order 10^2–10^3. The same tendency has been detected by molecular dynamics simulations in a three-dimensional (3D) binary mixture with $N = 500$ particles [4] and in a two-dimensional (2D) binary mixture with $N = 1024$ [5]. In our recent 3D simulation with $N = 10^4$ [6], η and D both varied over four decades and the power law behavior $D \propto \eta^{-0.75}$ has been observed. Many authors have attributed the origin of the breakdown to heterogeneous coexistence of relativity active and inactive regions, among which the local diffusion constant is expected to vary significantly [2,3,7–9]. The aim of this paper is to demonstrate via molecular dynamics (MD) simulation that the diffusivity of the particles is indeed heterogeneous on time scales shorter than the structural or α relaxation time τ_α but becomes homogeneous on time scales much longer than τ_α.

A number of recent MD simulations have detected dynamic heterogeneities in supercooled model binary mixtures [10–14]. That is, rearrangements of particle configurations in glassy states are cooperative, involving many molecules, owing to configuration restrictions [15]. In particular, we have examined bond breakage processes among adjacent particle pairs and found that the broken bonds in an appropriate time interval ($\sim\tau_\alpha$) are very analogous to the critical fluctuations in Ising spin systems with their structure factor being excellently fitted to the Ornstein-Zernike form [6,12]. The correlation length ξ thus obtained is related to the α relaxation time τ_α via the dynamic scaling law, $\tau_\alpha \sim \xi^z$, with $z = 4$ in 2D and $z = 2$ in 3D. The heterogeneity structure in the bond breakage is essentially the same as that in jump motions of particles from cages or that in the local diffusivity, as will be discussed below. However, there is no theory on these large-scale heterogeneities.

Our 3D binary mixture is composed of two atomic species, 1 and 2, with $N_1 = N_2 = 5000$ particles with the system linear dimension $L = V^{1/3}$ being fixed at $23.2\sigma_1$ [16]. They interact via the soft-core potentials $v_{ab}(r) = \epsilon(\sigma_{ab}/r)^{12}$ with $\sigma_{ab} = (\sigma_a + \sigma_b)/2$, where r is the distance between two particles and $a, b \in \{1, 2\}$. The interaction is truncated at $r = 3\sigma_1$. The mass ratio is $m_2/m_1 = 2$. The size ratio is $\sigma_2/\sigma_1 = 1.2$, which is known to prevent crystallization [10,16]. No tendency of phase separation is detected at least in our computation times. We fix the particle density at a very high value of $(N_1 + N_2)/V = 0.8/\sigma_1^3$, so the particle configurations are severely restricted or jammed. We will measure space and time in units of σ_1 and $\tau_0 = (m_1\sigma_1^2/\epsilon)^{1/2}$. The temperature T will be measured in units of ϵ/k_B, and the viscosity η in units of $\epsilon\tau_0/\sigma_1^3$. The time step $\Delta t = 0.005$ is used, and very long annealing times (2.5×10^5 for $T = 0.267$) are chosen in our case. For $T \geq 0.267$, no appreciable aging (slow equilibration) effect is detected in various quantities such as the pressure or the density time correlation function, whereas at the lowest temperature, $T = 0.234$, a small aging effect remains in the density time correlation function.

Let us consider the incoherent density correlation function, $F_s(q,t) = \langle \sum_{j=1}^{N_1} \exp[i\boldsymbol{q} \cdot \Delta\boldsymbol{r}_j(t)] \rangle / N_1$ for the particle species 1, where $\Delta\boldsymbol{r}_j(t) = \boldsymbol{r}_j(t) - \boldsymbol{r}_j(0)$ is the displacement vector of the jth particle. This function may be introduced also in shear flow [6]. The α relaxation time τ_α is then defined by $F_s(q, \tau_\alpha) = e^{-1}$ at $q = 2\pi$ for various T (and the shear rate $\dot\gamma$).

We also calculate the coherent time correlation function, $S_{11}(q,t) = \langle n_1(\boldsymbol{q},t) n_1(-\boldsymbol{q},0)\rangle$, where $n_1(\boldsymbol{q},t) = \sum_{j=1}^{N_1} \exp[i\boldsymbol{q}\cdot\boldsymbol{r}_j(t)]$ is the Fourier component of the density fluctuations of the particle species 1. The decay profiles of $S_{11}(q,t)$ at its first peak wave number $q = q_m \sim 2\pi$ and $F_s(q,t)$ at $q = 2\pi$ nearly coincide in the whole time region studied ($t < 2 \times 10^5$) within 5%. Hence, $S_{11}(q_m,\tau_\alpha)/S_{11}(q_m,0) \cong e^{-1}$ holds for any T in our simulation. Such agreement is not obtained for other wave numbers, however. These results are consistent with those for a Lennard-Jones binary mixture [17]. Furthermore, some neutron-spin-echo experiments [18] showed that the decay time of $S_{11}(q_m,t)$ is nearly equal to the stress relaxation time and as a result the viscosity η is of order τ_α. In agreement with this experimental result, we obtain a simple linear relation in our simulations:

$$\tau_\alpha \cong (A_\eta/q_m^2)\eta/T\,. \tag{1}$$

The coefficient A_η is close to 2π in our system. Figure 1 shows that Eq. (1) is valid over a wide range of τ_α. Here, we may define a q-dependent relaxation time τ_q by $F(q,\tau_q) = e^{-1}$. Thus, particularly at the peak wave number $q = q_m$, the effective diffusion constant defined by $D_q \equiv 1/q^2\tau_q$ is given by the Stokes-Einstein form even in highly supercooled liquids.

However, notice that the usual diffusion constant is the long wavelength limit, $D = \lim_{q\to 0} D_q$. It is usually calculated from the mean square displacement, $\langle[\Delta\boldsymbol{r}(t)]^2\rangle = \langle\sum_{j=1}^{N_1}[\Delta\boldsymbol{r}_j(t)]^2\rangle/N_1$. The crossover of this quantity from the plateau behavior arising from motions in transient cages to the diffusion behavior $6Dt$ has been found to take place around $t \sim 0.1\tau_\alpha$ [6]. In Fig. 2, we plot $D\tau_\alpha$ versus τ_α, which clearly indicates breakdown of the Stokes-Einstein relation in agreement with the experimental trend.

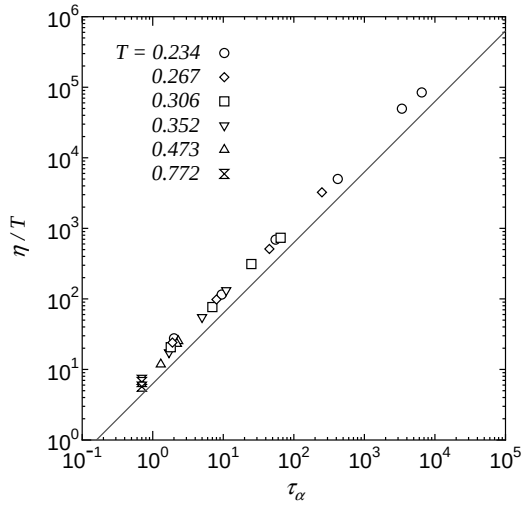

FIG. 1. η/T versus τ_α at various temperatures obtained from nonequilibrium MD in shear flow [6]. The straight line represents $\eta/T = 2\pi\tau_\alpha$.

To examine the diffusion process in more detail, we consider the van Hove self-correlation function, $G_s(r,t) = \langle\sum_{j=1}^{N_1}\delta(\Delta\boldsymbol{r}_j(t) - \boldsymbol{r})\rangle/N_1$. Then

$$F_s(q,t) = \int_0^\infty dr\,\frac{\sin(qr)}{qr}\,4\pi r^2 G_s(r,t) \tag{2}$$

is the 3D Fourier transformation of $G_s(r,t)$. At the peak wave number $q = 2\pi$, the integrand in Eq. (2) vanishes at $r = 1$, and the integral in the region $r < 1$ is confirmed to dominantly determine the decay of $F_s(2\pi,t)$. On the other hand, the mean square displacement,

$$\langle[\Delta\boldsymbol{r}(t)]^2\rangle = \int_0^\infty dr 4\pi r^4 G_s(r,t)\,, \tag{3}$$

is determined by the particle motions out of the cages for $t \gtrsim \tau_\alpha$ in glassy states. In Fig. 3, we display $4\pi r^4 G_s(r,\tau_\alpha)$ versus r at zero shear, where $\tau_\alpha = 3.2$ and 2000 for $T = 0.473$ and 0.267, respectively. These curves may be compared with the Gaussian (Brownian motion) result, $(2/\pi)^{1/2}\ell^{-3}r^4\exp(-r^2/2\ell^2)$, where $3\ell^2 = 6D_{\rm SE}\tau_\alpha = 3/2\pi^2$ is the Stokes-Einstein mean square displacement. Because the areas below the curves give $6D\tau_\alpha$, we recognize that the particle motions over large distances $r > 1$ are much enhanced at low T, leading to the violation of the Stokes-Einstein relation.

We then visualize the heterogeneity of the diffusivity. To this end, we pick up mobile particles of the species 1 with $|\Delta\boldsymbol{r}_j(t)| > \ell_c$ in a time interval $[t_0, t_0 + t]$ and number them as $j = 1,\ldots,N_m$. Here, ℓ_c is defined such that the sum of $\Delta\boldsymbol{r}_j(t)^2$ of the mobile particles is 66% of the total sum ($\cong 6DtN_1$ for $t \gtrsim 0.1\tau_\alpha$). In Fig. 4, these particles are drawn as spheres with radii

$$a_j(t) \equiv |\Delta\boldsymbol{r}_j(t)|/\sqrt{\langle[\Delta\boldsymbol{r}_j(t)]^2\rangle} \tag{4}$$

located at $\boldsymbol{R}_j(t) \equiv \frac{1}{2}[\boldsymbol{r}_j(t_0) + \boldsymbol{r}_j(t_0 + t)]$ in three time

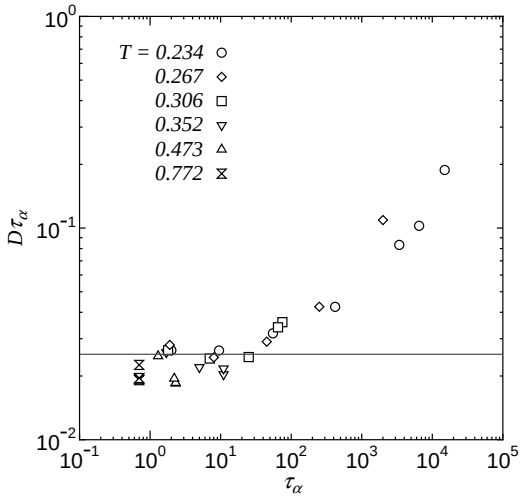

FIG. 2. $D\tau_\alpha$ versus τ_α. The solid line represents the Stokes-Einstein value $D_{\rm SE}\tau_\alpha = (2\pi)^{-2}$ arising from Eq. (1).

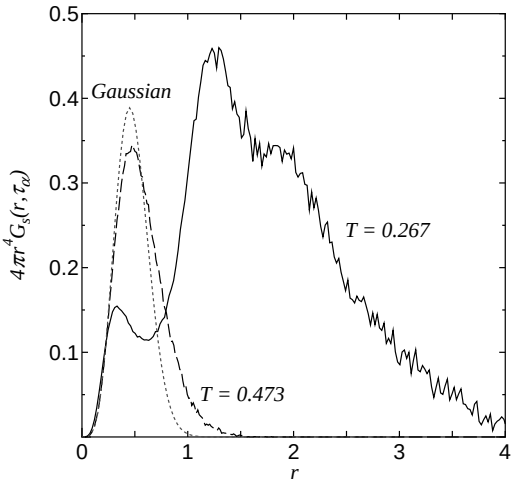

FIG. 3. $4\pi r^4 G_s(r,t)$ versus r at $t = \tau_\alpha$. The solid line is for $T = 0.267$ and the broken line is for $T = 0.473$. The dotted line represents the Brownian motion result. The peaks at $r \simeq 1.2$ and 2 in the solid line arise from hopping processes in our system at $T = 0.267$. Note that the areas below the curves give $6D\tau_\alpha$.

intervals: $[t_0, t_0 + 0.125\tau_\alpha]$ in 4(a), $[t_0, t_0 + \tau_\alpha]$ in 4(b), and $[t_0, t_0 + 10\tau_\alpha]$ in 4(c). The lower cutoff ℓ_c and the mobile particle number N_m increase with increasing t as 0.48 and 571 in 4(a), 1.3 and 725 in 4(b), and 2.9 and 1316 in 4(c), respectively. Here they approach the Gaussian results, $\ell_c = 0.403(t/\tau_\alpha)^{1/2}$ and $N_m = 1800$, for $t \gg \tau_\alpha$. In our case, the ratio of the second moments $c_2 \equiv \sum_{j=1}^{N_m} a_j(t)^2 / \sum_{j=1}^{N_1} a_j(t)^2$ is held fixed at 0.66 independently of t, while the ratio of fourth moments $c_4 \equiv \sum_{j=1}^{N_m} a_j(t)^4 / \sum_{j=1}^{N_1} a_j(t)^4$ turns out to be close to 1 as $c_4 = 0.97$ in 4(a), 0.92 in 4(b), and 0.90 in 4(c). We can see that the large scale heterogeneities in 4(a) and 4(b) are much weakened in 4(c) and that the areas of the spheres have the largest variance in 4(a). In fact, the variance defined by $\mathcal{V} \equiv N_m \sum_{j=1}^{N_m} a_j(t)^4 / [\sum_{j=1}^{N_m} a_j(t)^2]^2 - 1$ is 0.94 in 4(a), 0.41 in 4(b), and 0.32 in 4(c). Here, $c_4 \to 0.833$ and $\mathcal{V} \to 0.13$ for $t \gg \tau_\alpha$. The above result is consistent with the fact that the non-Gaussian parameter $A_2 \equiv 3\langle \Delta \boldsymbol{r}(t)^4 \rangle / 5\langle \Delta \boldsymbol{r}(t)^2 \rangle^2 - 1 = 3N_1 \langle \sum_{j=1}^{N_1} a_j(t)^4 \rangle / 5[\langle \sum_{j=1}^{N_1} a_j(t)^2 \rangle]^2 - 1$ takes a maximum value of 3.1 at $t \cong 0.125\tau_\alpha$ at this temperature. This is because the statistical average of $\mathcal{V}$ (taken over many initial times t_0) is related to $A_2(t)$ by $\langle \mathcal{V} \rangle \cong (5\langle c_4 \rangle \langle N_m \rangle / 3c_2^2 N_1)[1 + A_2(t)] - 1$, where the deviations $c_4 - \langle c_4 \rangle$ and $N_m / \langle N_m \rangle - 1$ are confirmed to be very small for large N_1 and are thus neglected. We may also conclude that the significant rise of $A_2(t)$ in glassy states originates from the heterogeneity in accord with some experimental interpretations [19].

Furthermore, we consider the Fourier component of the *diffusivity* density defined by

$$\mathcal{D}_{\boldsymbol{q}}(t_0, t) \equiv \sum_{j=1}^{N_m} a_j(t)^2 \exp[-i\boldsymbol{q} \cdot \boldsymbol{R}_j(t)], \qquad (5)$$

which depends on the initial time t_0 and the final time $t_0 + t$. The correlation function $S_{\mathcal{D}}(q, t, \tau) = \langle \mathcal{D}_{\boldsymbol{q}}(t_0 + \tau, t) \mathcal{D}_{-\boldsymbol{q}}(t_0, t) \rangle$ is then obtained after averaging over many initial states. We confirm that $S_{\mathcal{D}}(q, t, \tau)$ tends to its long wavelength limit for $q \lesssim \xi^{-1}$, where ξ coincides with the correlation length of the heterogeneity structure of the bond breakage [6,12]. As the difference τ of the initial times increases with fixed $t = \tau_\alpha$, $S_{\mathcal{D}}(q, \tau_\alpha, \tau)$ relaxes as $\exp[-(\tau/\tau_h)^c]$ for $q \lesssim \xi^{-1}$, where $c \sim 0.5$ at $T = 0.267$ and $\tau_h \sim 3\tau_\alpha$ is the lifetime of the heterogeneity structure. The two-time correlation function among the broken bond density [6,12] also relaxes with τ_h in the same manner.

We naturally expect that the distribution of the particle displacement $\Delta \boldsymbol{r}_j(t)$ in the active regions should be characterized by the local diffusion constant $D(\boldsymbol{x}, t)$ dependent on the spatial position $\boldsymbol{x} = (x, y, z)$ and the

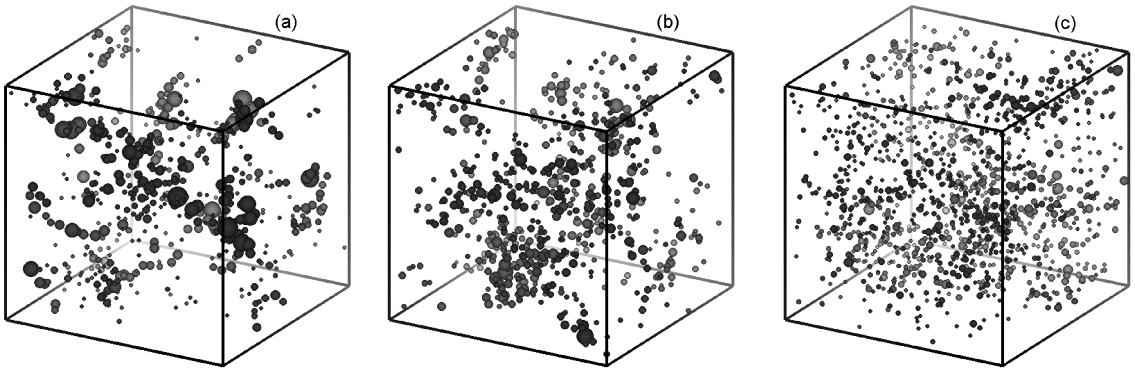

FIG. 4. Mobile particles of the species 1 at $T = 0.267$. The time interval t is $0.125\tau_\alpha$ in (a), τ_α in (b), and $10\tau_\alpha$ in (c). The radii of the spheres are $|\Delta \boldsymbol{r}_j(t)| / \sqrt{\langle (\Delta \boldsymbol{r}(t))^2 \rangle}$ and the centers are at $\frac{1}{2}[\boldsymbol{r}_j(t^0) + \boldsymbol{r}_j(t^0 + t)]$. The system linear dimension is $L = 23.2$. The darkness of the spheres represents the depth in the 3D space. The heterogeneity is significant at $0.125\tau_\alpha$ and τ_α but is much decreased at $10\tau_\alpha$.

time interval t. The van Hove correlation function $G_s(r,t)$ may then be expressed as the spatial average of a local function $G_s(\boldsymbol{x},r,t)$, which is given by $[4\pi D(\boldsymbol{x},t)t]^{-3/2}\exp[-r^2/4D(\boldsymbol{x},t)t]$. To check this conjecture, we plot the scaled function $\sqrt{6Dt}\,4\pi r^2 G_s(r,t)$ versus $r^* = r/\sqrt{6Dt}$ in Fig. 5. The areas below the curves are fixed at 1. At relatively short times $t \lesssim 3\tau_\alpha$, the curves in the region $r \gtrsim 1$ or $r^* \gtrsim (6Dt)^{-1/2}$, which give dominant contributions to $\langle[\Delta\boldsymbol{r}(t)]^2\rangle$, tend to a master curve quite different from the rapidly decaying Gaussian tail. Note that in each curve the position of the peak at larger r^* corresponds to $r \cong 1$. This asymptotic law is consistent with the picture of the space-dependent diffusion constant in the active regions. It is also important that the heterogeneity structure remains unchanged in the time region $t \lesssim \tau_h \sim 3\tau_\alpha$. At longer times $t \gtrsim 10\tau_\alpha$, the curves approach the Gaussian form as can be seen in the inset of Fig. 5. Of course, $4\pi r^2 G_s(r,t)$ for $r < 1$ does not scale in the above manner, because it is the probability density of a tagged particle staying within a cage. This short-range behavior determines the decay of $F_s(2\pi,t)$ as noted below Eq. (2).

In conclusion, our MD simulations demonstrate that the diffusivity in supercooled liquids is spatially heterogeneous on time scales shorter than $3\tau_\alpha$, which leads to the breakdown of the Stokes-Einstein relation. The heterogeneity detected is essentially the same as that of the bond breakage in our previous work [6]. We should then investigate how the heterogeneity arises and influences observable quantities in more realistic glass-forming fluids with complex structures.

We thank T. Kanaya for helpful discussions. This work is supported by Grants in Aid for Scientific Research from the Ministry of Education, Science, and Culture. Calculations have been performed at the Supercomputer Laboratory, Institute for Chemical Research, Kyoto University.

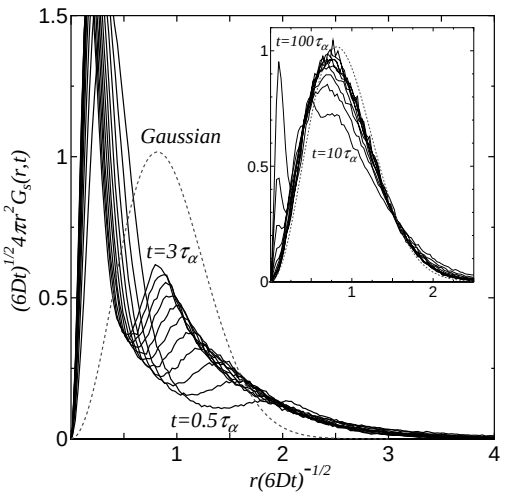

FIG. 5. A test of the scaling plot $\sqrt{6Dt}\,4\pi r^2 G_s(r,t)$ versus $r/\sqrt{6Dt}$ for $0.5\tau_\alpha < t < 3\tau_\alpha$ $[t = (0.5 + 0.25n)\tau_\alpha, n = 0,1,2,\ldots,10]$. The inset shows the curves at longer times, $10\tau_\alpha < t < 100\tau_\alpha$ $(t = 10n\tau_\alpha, n = 1,2,\ldots,10)$ where the heterogeneity effect is smoothed out. The dotted lines are the Gaussian form.

[1] M. D. Ediger, C. A. Angell, and S. R. Nagel, J. Phys. Chem. **100**, 13 200 (1996).
[2] F. Fujara, B. Geil, H. Sillescu, and G. Fleischer, Z. Phys. B **88**, 195 (1992); I. Chang *et al.*, J. Non-Cryst. Solids **172–174**, 248 (1994).
[3] M. T. Cicerone, F. R. Blackburn, and M. D. Ediger, Macromolecules **28**, 8224 (1995); M. T. Cicerone and M. D. Ediger, J. Chem. Phys. **104**, 7210 (1996).
[4] D. Thirumalai and R. D. Mountain, Phys. Rev. E **47**, 479 (1993).
[5] D. Perera and P. Harrowell, Phys. Rev. Lett. **81**, 120 (1988).
[6] R. Yamamoto and A. Onuki, Phys. Rev. E **58**, 3515 (1988). Here we define $F_s(q,t)$ in shear flow of the form, $\dot\gamma y e_x$, by setting $\Delta\boldsymbol{r}_j(t) = \boldsymbol{r}_j(t) - \dot\gamma\int_0^t dt' y_j(t') e_x - \boldsymbol{r}_j(0)$, where e_x is the unit vector in the x direction. Then $F_s(q,t)$ turns out to be almost independent of the angle of q. The viscosity and τ_α under shear satisfy Eq. (1) even in the non-Newtonian regime $\dot\gamma\tau_\alpha > 1$.
[7] F. H. Stillinger and A. Hodgdon, Phys. Rev. E **50**, 2064 (1994).
[8] G. Tarjus and D. Kivelson, J. Chem. Phys. **103**, 3071 (1995).
[9] C. Z.-W. Liu and I. Oppenheim, Phys. Rev. E **53**, 799 (1996).
[10] T. Muranaka and Y. Hiwatari, Phys. Rev. E **51**, R2735 (1995); T. Muranaka and Y. Hiwatari, J. Phys. Soc. Jpn. **67**, 1982 (1998).
[11] M. M. Hurley and P. Harrowell, Phys. Rev. E **52**, 1694 (1995); D. N. Perera and P. Harrowell, Phys. Rev. E **54**, 1652 (1996).
[12] R. Yamamoto and A. Onuki, J. Phys. Soc. Jpn. **66**, 2545 (1997); Europhys. Lett. **40**, 61 (1997); A. Onuki and R. Yamamoto, J. Non-Cryst. Solids **235–237**, 34 (1998).
[13] W. Kob *et al.*, Phys. Rev. Lett. **79**, 2827 (1997); C. Donati *et al.*, Phys. Rev. Lett. **80**, 2338 (1998).
[14] A. I. Mel'cuk *et al.*, Phys. Rev. Lett. **75**, 2522 (1995); G. Johnson *et al.*, Phys. Rev. E **57**, 5707 (1998).
[15] G. Adam and J. H. Gibbs, J. Chem. Phys. **43**, 139 (1965).
[16] G. Bernu, Y. Hiwatari, and J. P. Hansen, J. Phys. C **18**, L371 (1985); B. Bernu, J. P. Hansen, Y. Hiwatari, and G. Pastore, Phys. Rev. A **36**, 4891 (1987); J. Matsui, T. Odagaki, and Y. Hiwatari, Phys. Rev. Lett. **73**, 2452 (1994).
[17] W. Kob and H. C. Andersen, Phys. Rev. E **52**, 4134 (1995).
[18] F. Mezei, W. Knaak, and B. Farago, Phys. Rev. Lett. **58**, 571 (1987); D. Richter, R. Frick, and B. Farago, Phys. Rev. Lett. **61**, 2465 (1988).
[19] R. Zorn, Phys. Rev. B **55**, 6249 (1997); T. Kanaya, I. Tsukushi, and K. Kaji, Prog. Theor. Phys. Suppl. **126**, 133 (1997).